JCTC Journal of Chemical Theory and Computation

Article

pubs.acs.org/JCTC

Why Quantum Coherence Is Not Important in the Fenna−Matthews−Olsen Complex

David M. Wilkins*

Physical and Theoretical Chemistry Laboratory, Oxford University, South Parks Road, Oxford, OX1 3QZ, United Kingdom

Nikesh S. Dattani*

Quantum Chemistry Laboratory, Department of Chemistry, Kyoto University, 606-8502, Kyoto, Japan

School of Materials Science and Engineering, Nanyang Technological University, Block N4.1, Nanyang Avenue, Singapore 639798

Supporting Information

ABSTRACT: We develop and present an improvement to the conventional technique for solving the Hierarchical Equations of Motion (HEOM), which can reduce the memory cost by up to 75% while retaining the same (or even better) convergence rate and accuracy. This allows for a full calculation of the population dynamics of the 24-site FMO trimer for long time scales with very little effort, and we present the first fully converged, exact results for the 7-site subsystem of the monomer, and for the full 24-site trimer. We then show where our exact 7-site results deviate from the approximation of Ishizaki and Fleming [A. Ishizaki and G. R. Fleming, *Proc. Natl. Acad. Sci. U.S.A.*, **2009**, *106*, 17255]. Our exact results are then compared to calculations using the incoherent Förster theory, and it is found that the time scale of energy transfer is roughly the same, regardless of whether or not coherence is considered. This means that coherence is not likely to improve the efficiency of the transfer. In fact, the incoherent theory often tends to overpredict the rates of energy transfer, suggesting that, in some cases, quantum coherence may actually slow the photosynthetic process.

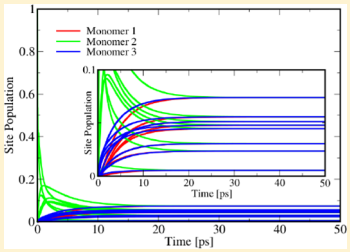

I. INTRODUCTION

There has been much excitement in recent years about the observation of surprisingly long-lived quantum coherence (the presence of nonzero off-diagonal elements in a quantum mechanical density matrix) in the excitation energy transfer in photosynthetic systems.[1−28] Since being first observed, it has been suggested that this coherence may be important for efficient transfer of the electronic excitation.[1−3,5,12,29,30]

Much of the study of this effect has focused on the Fenna−Matthews−Olson (FMO) complex,[32,33] which is found in green sulfur bacteria such as *C. tepidum* and *P. aestuarii*, and funnels excitation energy, collected by a light-harvesting chlorosome, toward a photosynthetic reaction center. The FMO complex comprises bacteriochlorophyll (BChl) pigments bound to a protein, and is a trimer, with each monomer containing eight BChl molecules (the existence of the eighth having been confirmed only relatively recently[34,35]). The FMO complex is an extremely popular system for both experimental and theoretical studies of energy transfer in photosynthesis, because of its small size and simplicity.

The two-dimensional (2D) electronic spectroscopy experiments of Engel et al.,[1] carried out on the FMO complex, showed long-lived quantum beating at cryogenic temperature (77 K). A follow-up theoretical study by Ishizaki and Fleming[2] at both 77 and 300 K suggested that quantum coherent energy transfer might also be observed in the complex at 300 K. Since then, long-lived quantum beating has indeed been observed in 2D spectroscopy experiments of the FMO complex at room temperature.[3] This coherence has been the subject of scores of recent theoretical studies of energy transfer in photosynthesis (for recent reviews of these studies, see refs 36−39).

However, the question of whether or not quantum coherence is important for the energy transfer is controversial. In particular, there have been many recent papers that question the nature of this coherence,[40−45] showing that classical theories can account for long-lived oscillations. Nonetheless, despite having previously been applied to energy transfer,[4,46−48] the incoherent Förster is dismissed in much of the literature as a predictive tool for the energy transfer dynamics, because of the fact that it neglects coherence.[49,50]

The existence of methods such as the Hierarchical Equations of Motion (HEOM), discussed in section II, allows the excitation energy transfer dynamics in the FMO complex to be simulated with numerically exact accuracy for a given Hamiltonian, meaning that the validity of approximate techniques can be tested. Comparing the predictions of Förster theory to those of the HEOM will allow us to evaluate whether or not quantum coherence is truly important in the energy transfer in the FMO complex. We will consider transfer at 300 K, since this is more relevant to the question of room-

Received: November 27, 2014

DOI: 10.1021/ct501066k
J. Chem. Theory Comput. XXXX, XXX, XXX−XXX

temperature coherence, and will look at electronic energy transfer throughout the entire 24-site trimer.

We first run a fully numerically exact calculation for the canonical model of the 7-site FMO subsystem, and we show that the approximation made by Ishizaki and Fleming in eq A2 of ref 50 leads to a noteworthy deviation from the exact dynamics. This means that various authors who have used the calculations from ref 50 as a benchmark to demonstrate the validity of their newly introduced methods (see, for example, refs 51−59) may not have been aware that their methods were, in fact, less or more accurate than they originally appeared, based on their comparison with ref 50.

We also look at long-time dynamics. Most simulations of the FMO complex published in the literature only look at the first 1 ps,[2,7,52,53,103] since coherence decays on a time scale of ∼400 fs. However, after the decay of coherence, the populations decay to a steady state,[53,54] and it is illuminating to look at both short- and long-time dynamics, in order to test the performance of Förster theory.

The fluorescence lifetime of the FMO complex is on the order of 1 ns,[60] and, in this work, the time scales of excitation energy transfer are found to be ∼15 ps. Since the energy transfer rate is thus more than 50 times faster than that of spontaneous emission, any loss of population to the latter process can be neglected. The time scale of excitation trapping at the reaction center has been reported to be on the order of picoseconds, based on the time taken for equilibrium to be reached.[61] While an explicit treatment of the reaction center would give us the best idea of the efficiency of excitation transfer in the two methods, we can certainly get a very good idea of how these compare by looking at the transfer rates.

The remainder of this paper is set out as follows: Section II introduces the model used to describe excitation energy transfer, as well as the exact HEOM and approximate Förster theory. Section III compares the energy transfer dynamics predicted by the coherent and incoherent theories, and a conclusion is presented in section IV.

II. THEORY

In the model that we will use to describe the FMO complex,[2,52] we treat each BChl molecule as having two electronic energy levels, and denote the state in which BChl j is in its excited state (and all others are in their ground states) by $|j\rangle$. Then, the so-called system Hamiltonian for N BChl sites is

$$\hat{H}_S = \sum_{j=1}^{N} \epsilon_j |j\rangle\langle j| + \sum_{i=1}^{N-1} \sum_{j=i+1}^{N} J_{ij}(|i\rangle\langle j| + |j\rangle\langle i|) \tag{1a}$$

where ϵ_j is the energy of site j and J_{ij} is the dipolar coupling between sites i and j. Since we want to treat $\hat{H}_S$ as an open quantum system, each site is associated with a phonon bath consisting of the vibrations of the BChl molecule and the surrounding protein. Each bath has an infinite number of oscillators, and the bath Hamiltonian is

$$\hat{H}_B = \sum_{j=1}^{N} \sum_{\kappa=1}^{\infty} \left(\frac{\hat{p}_{j\kappa}^{\,2}}{2m_{j\kappa}} + \frac{1}{2} m_{j\kappa} \omega_{j\kappa}^{\,2} \hat{q}_{j\kappa}^{\,2} \right) \tag{1b}$$

where $\hat{q}_{j\kappa}$ is the coordinate of phonon mode κ associated with site j, $\hat{p}_{j\kappa}$ is its momentum, $m_{j\kappa}$ its mass, and $\omega_{j\kappa}$ its angular frequency. Finally, there is a vibronic interaction between each site and its bath, given by the system−bath coupling Hamiltonian:

$$\hat{H}_{SB} = -\sum_{j=1}^{N} \hat{V}_j \hat{u}_j \tag{1c}$$

Here, $\hat{V}_j \equiv |j\rangle\langle j|$, and $\hat{u}_j = \sum_\kappa g_{j\kappa} \hat{q}_{j\kappa}$, with $g_{j\kappa}$ describing the strength of the coupling of mode κ to site j. The total Hamiltonian for the FMO complex then is given by

$$\hat{H} = \hat{H}_S + \hat{H}_B + \hat{H}_{SB} \tag{2}$$

The bath has an infinite number of degrees of freedom, but since we are not interested in the dynamics of the bath degrees of freedom, we can average over them. The reduced (system) density operator is defined as a trace over the bath degrees of freedom in the total density operator $\hat{\rho}_{TOT}(t)$:

$$\hat{\rho}(t) = \mathrm{tr}_B[\hat{\rho}_{TOT}(t)] \tag{3}$$

For convenience, we take the initial density matrix to be factored as $\hat{\rho}_{TOT}(t) = \hat{\rho}_S(0) \otimes \hat{\rho}_B$, where $\hat{\rho}_S(0)$ is a system density matrix and $\hat{\rho}_B$ is the equilibrium density matrix for the bath. Since the completion of this work, Tanimura has developed a method to address correlated initial conditions within the HEOM.[64]

The influence of the bath on the system can be fully characterized by the spectral density $J_j(\omega)$ for the phonons coupled to site j:

$$J_j(\omega) = \sum_\kappa \frac{g_{j\kappa}^{\,2}}{2m_{j\kappa}\omega_{j\kappa}} \delta(\omega - \omega_{j\kappa}) \tag{4}$$

In addition, the bath correlation function $\alpha_j(t)$ is defined such that

$$\alpha_j(t_1, t_2) = \alpha_j(t_1 - t_2) = \langle \tilde{u}_j(t_1)\tilde{u}_j(t_2)\rangle_\beta$$

where $\langle\cdot\rangle_\beta$ represents a thermal average over the bath degrees of freedom, and

$$\tilde{u}_j(t) = e^{i\hat{H}_B t/\hbar} \hat{u}_j e^{-i\hat{H}_B t/\hbar}$$

This function is related to the spectral density by the expression

$$\alpha_j(t) = \int_0^\infty J_j(\omega) \left(\coth\left(\frac{\beta\hbar\omega}{2}\right)\cos(\omega t) - i\sin(\omega t) \right) d\omega \tag{5}$$

In the remainder of this paper, we will write the correlation function as a sum of exponentials:

$$\alpha_j(t) = \sum_k^K p_{jk} e^{-\gamma_{jk} t} \tag{6}$$

with p_{jk} and γ_{jk} defined by the Padé decomposition, which was first introduced in ref 62 and explained in more detail in ref 63.

We now introduce the two methods used in this paper to calculate the reduced density operator dynamics for this system.

A. Hierarchical Equations of Motion. The HEOM methodology was originally developed by Tanimura[65,66] and since then has been used in various studies, for example (but not limited to) applications in Wigner space,[89−91] multidimensional spectroscopy,[68−74] rate theory,[75] and coupled oscillators.[76] Applications with low-temperature corrections began in Refs. [77] and [78], and various truncation schemes have been used to improve the efficiency of the algorithm.[65,66,79,80] It

DOI: 10.1021/ct501066k
J. Chem. Theory Comput. XXXX, XXX, XXX−XXX

has also motivated advancements in spectral density decompositions,[70,81−86] and recently it has been implemented on GPUs.[74,87] After the completion of this work, still more improvements to the technique have been made.[88] The HEOM give a numerically exact method for calculating the dynamics of the reduced density operator $\hat{\rho}(t)$, placing it at the top of a hierarchy of auxiliary density matrices (ADOs), denoted $\hat{\rho}_{\mathbf{n}}(t)$. $\mathbf{n}$ is a $J \times K$ matrix, with J the number of baths and K the number of exponential terms in eq 6; an element of $\mathbf{n}$ is denoted as n_{jk}; all of these elements must be non-negative.

Level n of the hierarchy consists of all ADOs for which

$$\sum_{j=1}^{J}\sum_{k=1}^{K} n_{jk} = n, \quad n > 0 \tag{7}$$

and the matrix with $\mathbf{n} = \mathbf{0}$ is the reduced density operator. In principle, the hierarchy has an infinite number of layers; however, in practice, a finite number of levels is sufficient for converged results. The equation of motion for an ADO can be expressed as[50,54]

$$\begin{aligned}\frac{\mathrm{d}}{\mathrm{d}t}\hat{\rho}_{\mathbf{n}}(t) = &-\frac{i}{\hbar}[\hat{H}_{\mathrm{S}}, \hat{\rho}_{\mathbf{n}}(t)] - \sum_{j=1}^{J}\sum_{k=1}^{K} n_{jk}\gamma_{jk}\hat{\rho}_{\mathbf{n}}(t) \\ &+ i\sum_{j=1}^{J}\sum_{k=1}^{K}\left([\hat{V}_j, \hat{\rho}_{\mathbf{n}_{jk+}}(t)] + \frac{1}{\hbar}n_{jk}p_{jk}\hat{V}_j\hat{\rho}_{\mathbf{n}_{jk-}}(t)\right. \\ &\left. + \frac{1}{\hbar}n_{jk}p_{jk}^{*}\hat{\rho}_{\mathbf{n}_{jk-}}(t)\hat{V}_j\right)\end{aligned} \tag{8}$$

where $\hat{\rho}_{\mathbf{n}_{jk\pm}}(t)$ is indexed by a matrix almost identical to that of $\hat{\rho}_{\mathbf{n}}(t)$, but with the element n_{jk} replaced by $n_{jk} \pm 1$. Thus, each ADO is coupled to operators in the level above and in the level below it in the hierarchy. If $n_{jk} = 0$, then $\hat{\rho}_{\mathbf{n}_{jk-}}(t) = 0$, and, similarly, if $\hat{\rho}_{\mathbf{n}}(t)$ is on the highest level of the hierarchy, then $\hat{\rho}_{\mathbf{n}_{jk+}}(t) = 0$ for all j and k.

Rather than solving this set of coupled differential equations using the traditional RK4 method, we used the fact that the equations are linear in the elements of the ADOs. If $\underline{\varrho}(t)$ is a vector containing all of these elements, then the HEOM can be written in terms of a linear transformation T:

$$T: \quad \underline{\varrho}(t) \rightarrow \frac{\mathrm{d}}{\mathrm{d}t}\underline{\varrho}(t) \tag{9}$$

Since T is time-independent, eq 9 has the formal solution

$$\underline{\varrho}(t + \Delta t) = \exp(T\Delta t)\underline{\varrho}(t) \tag{10}$$

Expanding this as a power series and including terms up to order $(\Delta t)^L$, where L is any integer, gives the approximation

$$\underline{\varrho}(t + \Delta t) = \sum_{l=0}^{L}\frac{(\Delta t)^l}{l!}T^l\underline{\varrho}(t) + O((\Delta t)^{L+1}) \tag{11}$$

where $T^l\underline{\varrho}(t)$ is short for the l^{th} derivative of $\underline{\varrho}(t)$, calculated using eq 8. This avoids calculating a matrix representation for T, which is potentially very large (although sparse). The algorithm we used to propagate $\underline{\varrho}(t)$ through time used a second vector, $\underline{\varrho}'$, for storage:

(1) Set $\underline{\varrho}' = \underline{\varrho}(t)$.
(2) Set $\underline{\varrho}(t+\Delta t) = \underline{\varrho}(t)$.
(3) For $l = 1$ to L:

- Set $\underline{\varrho}' = (\Delta t)T\underline{\varrho}'/l$
- Set $\underline{\varrho}(t+\Delta t) = \underline{\varrho}(t+\Delta t) + \underline{\varrho}'$

For $L = 4$, this method has the same order of convergence as the RK4 method. Since L can be varied, it can be optimized to give the most efficient use of memory: a smaller L requires a smaller time step, but fewer calculations of the time derivative. We found that $L = 2$ was the best compromise and gave the most-efficient time integration, with a time step of $\Delta t = 1$ fs giving converged results. In addition, using this method instead of RK4 can lead (depending on the implementation of the RK4 algorithm) to a decrease in memory usage from five vectors for each time-propagation step to only one, ρ', which could be a significant computational advantage. Since the time derivative of each ADO can be calculated independently, we parallelized the computation of these time derivatives. A runtime summary is provided in the Supporting Information.

B. Förster Theory. Förster theory was originally formulated to describe resonant energy transfer between two electronic states.[47,89] It is a perturbative theory, which works well if the magnitudes of the dipolar interactions $|J_{ij}|$ between sites are sufficiently smaller than the transition energies $|\epsilon_i - \epsilon_j|$ or the reorganization energy $\lambda_j = \int_0^\infty J_j(\omega)/\omega \, \mathrm{d}\omega$.[48] Since the transition energies are generally larger than the dipolar couplings in the FMO complex (in eq A1 in the Appendix, for example, the largest dipolar coupling, H_{12}, has a magnitude of 87.7 cm^{-1}, while $|\epsilon_1 - \epsilon_2| = 120$ cm^{-1}), we might expect this to be a reasonable approximation. In Förster theory, only the diagonal matrix elements of the reduced density operator (the site populations) are evolved through time, while the off-diagonal elements (coherences) are set equal to zero, meaning that the theory is incoherent.[90]

The theory involves a set of coupled rate equations for the site populations $\rho_{jj}(t) \equiv \langle j|\hat{\rho}(t)|j\rangle$:

$$\frac{\mathrm{d}}{\mathrm{d}t}\rho_{jj}(t) = \sum_{i=1}^{N}\sum_{j\neq i}^{N}(k_{i\rightarrow j}\rho_{ii}(t) - k_{j\rightarrow i}\rho_{jj}(t)) \tag{12}$$

with the transfer rate $k_{i\rightarrow j}$ given by[90]

$$k_{i\rightarrow j} = 2|J_{ij}|^2\Re\left(\int_0^\infty F_i^*(t)A_j(t)\,\mathrm{d}t\right) \tag{13}$$

where $\Re$ denotes the real part. $F_i(t)$ and $A_j(t)$ are the fluorescence and absorption line shape functions, respectively:

$$F_i(t) = \exp\left[-i\left(\frac{\epsilon_i}{\hbar} - \frac{\lambda_i}{\hbar}\right)t - g_i^*(t)\right] \tag{14a}$$

$$A_j(t) = \exp\left[-i\left(\frac{\epsilon_j}{\hbar} + \frac{\lambda_j}{\hbar}\right)t - g_j(t)\right] \tag{14b}$$

The line-broadening function is given as

$$g_{i,j}(t) = \frac{1}{\hbar^2}\int_0^t \mathrm{d}t_1\int_0^{t_1}\mathrm{d}t_2\alpha_{i,j}(t_2)$$

As explained by Yang and Fleming,[47,90] the fluorescence spectrum of site i is the Fourier transform of $F_i(t)$, and the absorption spectrum of site j is the Fourier transform of $A_j(t)$.

This represents a simple, easily implemented, and computationally inexpensive theory for incoherent excitation energy transfer, and, in section III, the comparison between the two theories will give an idea of how well the incoherent theory can predict the energy transfer dynamics.

DOI: 10.1021/ct501066k
J. Chem. Theory Comput. XXXX, XXX, XXX−XXX

III. RESULTS

In order to simulate the exact and approximate energy transfer dynamics for the 24-site FMO trimer and for the 7-site subsystem, we first present the physical parameters which we will use; all of this data is found in the Appendix.

The 7-site model system Hamiltonian that we use is that of Adolphs and Renger,[97] which is popular in theoretical studies of this system.[2,38,52,91−96,98] The parameters in this model are given in eq A1.

For the 24-site calculations, we follow the study by Ritschel et al.,[52] using the Hamiltonian given in eqs A2, with two sets of site energies as in eq A2-c: those of Olbrich et al. (OLB)[99] and those of Schmidt am Busch et al. (SAB).[35]

The spectral density chosen is the Lorentz−Drude/Debye spectral density:

$$J(\omega) = \frac{2}{\pi}\left(\frac{\lambda\gamma\omega}{\gamma^2 + \omega^2}\right) \tag{15}$$

with λ = 35 cm^{-1} and γ = 0.02 fs^{-1} (with the same spectral density used for every site). These parameters are used in the most popular benchmark study of energy transfer in the FMO,[2] which used this form for the spectral density, because it had been used successfully in the analyses of several experiments (in particular, refs 100−102). Using the Padé approximant to the Bose−Einstein function in the definition of $\alpha_j(t)$ represents $\alpha_j(t)$ in the form of eq 6.[63] At 300 K, convergence was obtained with two terms, with the values of the p_{jk} and the γ_{jk} given by eq A4 in the Appendix.

Since BChl molecules 1, 6, and 8 are closest to the chlorosome, it is these that are most likely to be excited initially, and so the simulations are started with excitation on one of these three sites. In each of the results shown, the populations of several sites are omitted, as they remain small throughout the simulation.

We begin by showing our numerically exact calculations on the full 24-site FMO trimer, in Figure 1. It is interesting to note

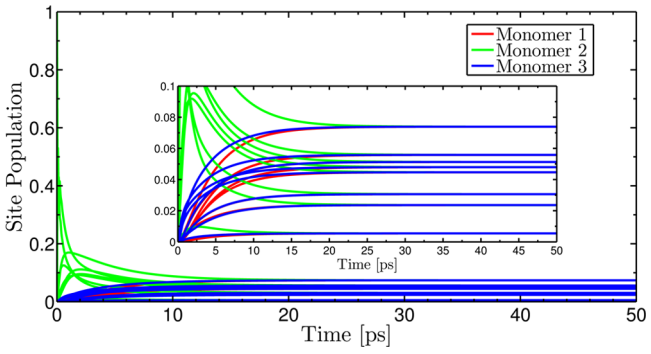

Figure 1. Numerically exact dynamics for the full 24-site trimer up to the steady state at 300 K, using γ = 0.02 fs^{-1} and λ = 35 cm^{-1}, with the Lorentz-Drude spectral density (using the 2-term Padé series of eq A4) and 4 levels of the hierarchy. Each color represents a particular monomer, as indicated in the legend.

that, regardless of which monomer was initially excited, all monomers are equally populated at equilibrium, and the population distribution is the same in each monomer. This is a consequence of the 3-fold rotational symmetry of the FMO complex, in which we see that, for a given site, the population at long times is the same on each monomer, regardless of which one was initially excited.

A. 7-Site System. Figure 2 compares the population dynamics at 77 K, after convergence is achieved with respect to

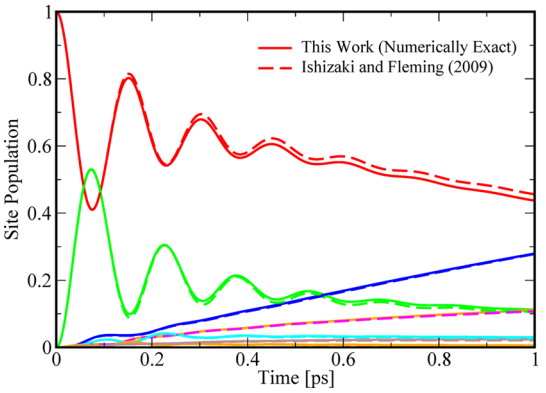

Figure 2. Comparison of HEOM results with full bath correlation function (solid lines) and those of ref 2 (dashed lines), with the bath correlation function approximated by one exponential and a delta function. In both cases, calculations were carried out at 77 K, using λ = 0.02 fs^{-1} and λ = 35 cm^{-1}, with the Lorentz-Drude spectral density and 5 levels of the hierarchy. The solid lines used the 3-term Padé series of eq A3.

the number of exponentials used to represent $\alpha(t)$ (three exponentials were used here, the numerical values for which are given in eq A3 in the Appendix), with the population dynamics presented by Ishizaki and Fleming in ref 2; these were for the same parameters, but with $\alpha(t)$ truncated as described by the approximation shown in eq A2 of their paper.[2] Therefore, the results we present here are the first numerically exact calculations for energy transfer in the FMO complex. The difference is expected to be even larger at lower temperatures, where more exponentials are required.

In Figure 3, we compare our fully converged dynamics, obtained using the HEOM, with incoherent Förster theory for the 7-site model at 300 K, with initial excitation on sites 1 and 6, showing both the short-time and longer-time dynamics. The HEOM results were obtained with two exponential terms in eq 6 (i.e., K = 2; the numerical values for these terms are given by eq A4 in the Appendix) and five layers of the hierarchy, which we found to be sufficient to fully converge the dynamics. The Förster theory calculations used the same bath correlation function, with K = 2.

Looking at the results of Förster theory, we see that despite not explicitly considering the off-diagonal elements of the density matrix, it still does surprisingly well: for the upper panels of Figure 3, in which site 1 is initially excited, the incoherent theory gives a very good prediction of the transfer rates, steady-state populations, and time scale on which the steady state is reached.

The lower panels of Figure 3, where site 6 is excited initially, show a somewhat less impressive comparison between the two methods: the steady-state populations are, naturally, independent of which site was populated at the beginning of the calculation, and therefore are matched just as well as in the upper panels, and the time scale on which the steady-state was reached is also captured well, but the transfer rates at short times are predicted quite poorly by Förster theory. However, the rates are overpredicted, which is contrary to popular opinion:[1−3,5,12] site 3, which is nearest to the reaction center, is predicted to have a greater population before ∼2.5 ps in the

DOI: 10.1021/ct501066k
J. Chem. Theory Comput. XXXX, XXX, XXX−XXX

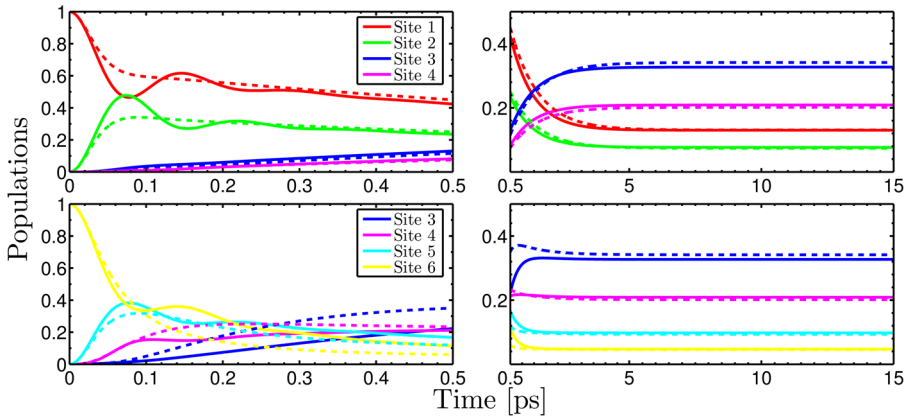

Figure 3. Comparison of HEOM (solid lines) and Förster theory (dashed lines) dynamics for the 7-site subsystem. The top row corresponds to initial excitation on site 1, and the bottom row corresponds to initial excitation on site 6. The left-hand column focuses on short-time dynamics, and the right-hand column shows the longer-time dynamics. These calculations were carried out at 300 K, using $\gamma = 0.02$ fs^{-1} and $\lambda = 35$ cm^{-1}, with the Lorentz-Drude spectral density (using the 3-term Padé series of eq A3) and 5 levels of the hierarchy.

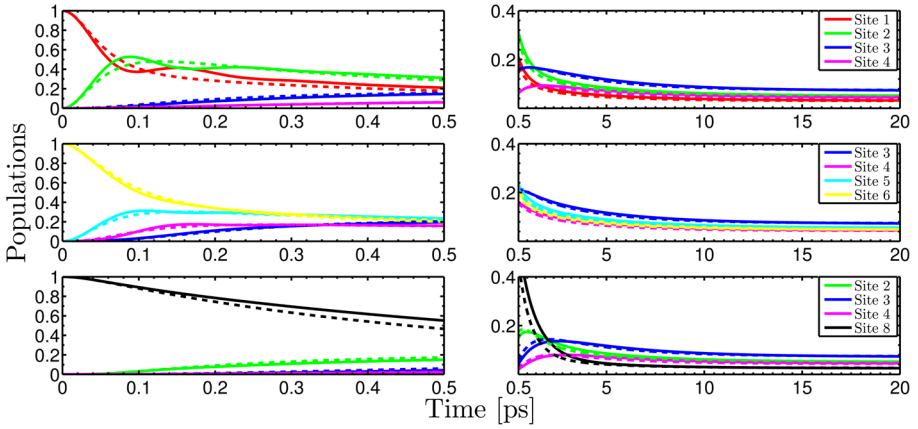

Figure 4. Comparison of HEOM (solid lines) and Förster theory (dashed lines) dynamics for the monomer, with the full 24-site system considered, with OLB site energies. The top row corresponds to initial excitation on site 1, the middle row corresponds to initial excitation on site 6 and the bottom row corresponds to initial excitation on site 8. The left-hand column shows short-time dynamics, and the right-hand column shows long-time dynamics. These calculations were carried out at 300 K, using $\gamma = 0.02$ fs^{-1} and $\lambda = 35$ cm^{-1}, with the Lorentz-Drude spectral density (using the 2-term Padé series of eq A4) and 4 levels of the hierarchy.

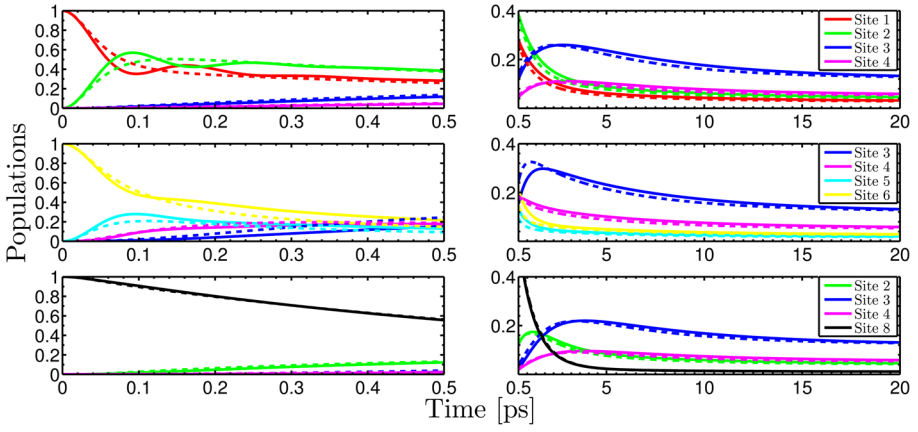

Figure 5. Comparison of HEOM (solid lines) and Förster theory (dashed lines) dynamics for the monomer with the initial excitation, with the full 24-site system considered, with SAB site energies. The top row corresponds to initial excitation on site 1, the middle row corresponds to initial excitation on site 6 and the bottom row corresponds to initial excitation on site 8. The left-hand column shows short-time dynamics, and the right-hand column shows long-time dynamics. These calculations were carried out at 300 K, using $\gamma = 0.02$ fs^{-1} and $\lambda = 35$ cm^{-1}, with the Lorentz-Drude spectral density (using the 2-term Padé series of eq A4) and 4 levels of the hierarchy.

incoherent theory than is seen in the exact results, which suggests that if transfer to the reaction center were to occur on this time scale, then incoherent transfer might be faster than coherent transfer.

DOI: 10.1021/ct501066k
J. Chem. Theory Comput. XXXX, XXX, XXX−XXX

B. 24-Site System. Almost all of the studies in the literature on energy transfer in the FMO complex as an open quantum system have only treated a subsystem of the full complex.[2,7,29,98,103] The only study of the full 24-site model to date was that of Ritschel et al.,[52] which used an approximate quantum master equation to simulate the dynamics up to 1 ps. However, one very interesting aspect that is new in the study of the full trimer is the emergence of a second time scale in the transfer dynamics. While the time scale for intramonomer energy transfer is expected (in a Förster-theory sense) to be on the order of $|\hbar/J_{ij}| \approx 400$ fs, where J_{ij} is an off-diagonal element taken from eq A2-b (specifically, between one of sites 1, 6, or 8 and its most strongly coupled neighbor), the time scale for intermonomer transfer will be on the order of $|\hbar/J'_{ij}| \approx 20$ ps, where J'_{ij} is an element from eq A2-d. Therefore, to get an idea of the dynamics of the 24-site model all the way to equilibrium, we have calculated the dynamics up to 20 ps.

Figure 4 compares the dynamics of HEOM and Förster theory for the 24-site model using the OLB site energies, for initial excitation on sites 1, 6, and 8 and for both short and longer time scales. Figure 5 repeats this comparison for the 24-site model using the SAB site energies. In each case, the bath correlation function contained two terms, and for the HEOM results, four levels of the hierarchy were used.

As in the 7-site system, the results of the HEOM calculations show coherences between sites 1 and 2 at short time scales for both site energies, but little coherence is observed between sites 5 and 6. When site 8 is initially excited, the transfer is incoherent; similar dynamics were reported at 77 K in ref 52, and at 300 K in the 8-site monomer in ref 29. In both Hamiltonians, despite the fact that site 8 is most strongly coupled to site 1, $J_{18} < \hbar|\epsilon_1 - \epsilon_8|$. The difference is much smaller in the OLB site energies than in the SAB energies, suggesting that, in the latter, coherence between these two sites will be minimal, although coherence may be seen in the former. In addition, the strong coupling between sites 1 and 2 means that excitation will flow to the second site before coherence could develop between site 8 and site 1.[52] Regardless of whether coherence occurs at short time scales, it is quenched by ~400 fs, and, as with the 7-site system, the dynamics then enters an exponential decay-like regime, finally reaching a steady state.

Once again, the predictions of Förster theory agree quite well with the exact dynamics: the general shapes of the population decays are followed with good accuracy, and both the time scales on which the steady state is reached, and the populations at this state, are captured—generally with better accuracy than for the 7-site system. The middle row in Figure 5, in which the SAB Hamiltonian is used and site 6 is initially excited, shows relatively poor agreement, as does the bottom row in Figure 4, in which the OLB Hamiltonian is used and site 8 is initially excited—but, once again, the transfer rates at short times are actually overpredicted by Förster theory. We have observed the same wherever the incoherent theory noticeably fails to match the exact results.

This failure of Förster theory, even in a case where the population dynamics initially appear to be incoherent, can be compared with the bottom row of Figure 5, in which the two theories are matched very well at short times. As described above, some coherence is possible between site 8 and site 1 with the OLB energies, and this could be the reason for the failure of the incoherent theory. However, overall, the performance of Förster theory is better for the full 24-site trimer than for the 7-site system.

IV. DISCUSSION

In this paper, we have presented a new method for solving the hierarchical equations of motion, and we have used this to perform the first numerically exact calculation for the full 24-site FMO trimer and the 7-site subsystem of a monomer. We have also compared these dynamics to the approximate, perturbative Förster theory. The upshot of our results is that, despite missing short-time oscillations, Förster theory provides quite a good description of energy transfer for the three popular models that we have considered. This is, perhaps, not surprising, because the applicability of the theory depends on the intersite coupling being smaller than the transition energy between sites, which is often the case here. In a recent review, Ishizaki et al. showed that, for a representative 2-site system, the energy transfer rate predicted by Förster theory should be similar to the exact transfer rate (see Figure 7 in ref 4) for a reorganization energy of $\lambda = 35$ cm^{-1}. This is consistent with the results that we have observed here for the 7- and 24-site systems.

The fact that, when the two theories give conflicting results at short times, Förster theory often has a tendency to overpredict excitation transfer rates, is interesting: it has previously been assumed that quantum coherence is harnessed to provide the efficient transfer observed, but we have seen that an incoherent theory can predict faster transfer. However, while studying the 24-site system is an improvement over previous studies, which only addressed smaller subsystems, the trapping of excitation at the reaction center is still omitted: this point is crucial, because without a better knowledge of the time scale of this trapping (which would require extending the Hamiltonian to include the reaction center), we cannot single out which method gives the most efficient transfer.

However, assuming that the rate of excitation trapping is on the order of picoseconds, we notice that it is on this time scale that the two theories begin to agree: even if the exact, coherent, energy transfer was more efficient, there would be only a modest difference in efficiencies between the two.

Förster theory is valid when the coupling between BChl sites is smaller than the transition energy between them. This means that, despite its simplicity, its reasonable predictions of transfer rates and long-time behavior greatly support our conclusion that the FMO complex does not seem to utilize coherence to provide efficient transfer after all.

APPENDIX

7-Site Hamiltonian. The 7-site Hamiltonian of Adolphs and Renger (energies shown in cm^{-1}) is given by[97]

$$\hat{H}_S = \begin{pmatrix} 410 & -87.7 & 5.5 & -5.9 & 6.7 & -13.7 & -9.9 \\ & 530 & 30.8 & 8.2 & 0.7 & 11.8 & 4.3 \\ & & 210 & -53.5 & -2.2 & -9.6 & 6.0 \\ & & & 320 & -70.7 & -17.0 & -63.3 \\ & & & & 480 & 81.1 & -1.3 \\ & & & & & 630 & 39.7 \\ & & & & & & 440 \end{pmatrix} \quad \text{(A1)}$$

24-Site Hamiltonian. The 24-site Hamiltonian has the form:

DOI: 10.1021/ct501066k
J. Chem. Theory Comput. XXXX, XXX, XXX−XXX

$$\hat{H}_S = \begin{pmatrix} \hat{h}_A & \hat{h}_B & \hat{h}_B^\dagger \\ \hat{h}_B^\dagger & \hat{h}_A & \hat{h}_B \\ \hat{h}_B & \hat{h}_B^\dagger & \hat{h}_A \end{pmatrix} \tag{A2-a}$$

with the intersite couplings (off-diagonal elements of $\hat{h}_A$) being given by[52]

$$\hat{h}_A = \begin{pmatrix} \hat{h}_{11} - 80.3 & 3.5 & -4.0 & 4.5 & -10.2 & -4.9 & 21.0 \\ & \hat{h}_{22} & 23.5 & 6.7 & 0.5 & 7.5 & 1.5 & 3.3 \\ & & \hat{h}_{33} & -49.8 & -1.5 & -6.5 & 1.2 & 0.7 \\ & & & \hat{h}_{44} & -63.4 & -13.3 & -42.2 & -1.2 \\ & & & & \hat{h}_{55} & 55.8 & 4.7 & 2.8 \\ & & & & & \hat{h}_{66} & 33.0 & -7.3 \\ & & & & & & \hat{h}_{77} & -8.7 \\ & & & & & & & \hat{h}_{88} \end{pmatrix} \tag{A2-b}$$

There are two sets of site energies (diagonal elements of $\hat{h}_A$): those of Olbrich et al.[99] (OLB) and those of Schmidt am Busch et al.[35] (SAB):

Element	$\hat{h}_{11}$	$\hat{h}_{22}$	$\hat{h}_{33}$	$\hat{h}_{44}$	$\hat{h}_{55}$	$\hat{h}_{66}$	$\hat{h}_{77}$	$\hat{h}_{88}$
OLB	186	81	0	113	65	89	492	218
SAB	310	230	0	180	405	320	270	505

(A2-c)

Finally, the intersite couplings $\hat{h}_B$ are given by[52]

$$\hat{h}_B = \begin{pmatrix} 1.0 & 3.0 & -0.6 & 0.7 & 2.3 & 1.5 & 0.9 & 0.1 \\ 1.5 & -0.4 & -2.5 & -1.5 & 7.4 & 5.2 & 1.5 & 0.7 \\ 1.4 & 0.1 & -2.7 & 5.7 & 4.6 & 2.3 & 4.0 & 0.8 \\ 0.3 & 0.5 & 0.7 & 1.9 & -0.6 & -0.4 & 1.9 & -0.8 \\ 0.7 & 0.9 & 1.1 & -0.1 & 1.8 & 0.1 & -0.7 & 1.3 \\ 0.1 & 0.7 & 0.8 & 1.4 & -1.4 & -1.5 & 1.6 & -1.0 \\ 0.3 & 0.2 & -0.7 & 4.8 & -1.6 & 0.1 & 5.7 & -2.3 \\ 0.1 & 0.6 & 1.5 & -1.1 & 4.0 & -3.1 & -5.2 & 3.6 \end{pmatrix} \tag{A2-d}$$

Bath Correlation Function. At 77 K, the integral in eq 5 is evaluated for the Drude-Lorentz/Debye spectral density using the [1/2] Padé series for the Bose−Einstein function,[62,63]

$$f_{\text{Bose}}(\beta\hbar\omega) = (1 - e^{-\beta\hbar\omega})^{-1}$$

giving three exponential terms in eq 6. The coefficients p_{jk} and γ_{jk} in this equation are

k	p_{jk} ($\text{cm}^{-1}\,\text{fs}^{-1}$)	γ_{jk} (fs^{-1})
1	0.4574−0.7000i	0.0200
2	0.5090	0.0636
3	0.8658	0.1966

(A3)

At 300 K, a [0/1] Padé series was used, giving two exponential terms in eq 6. The coefficients p_{jk} and γ_{jk} in this case are

k	p_{jk} ($\text{cm}^{-1}\,\text{fs}^{-1}$)	γ_{jk} (fs^{-1})
1	2.6897−0.7000i	0.0200
2	0.9076	0.3042

(A4)

The Padé parameters used to test convergence are included in the Supplementary Information.

■ ASSOCIATED CONTENT

Supporting Information

Summary of run-time and memory costs for our HEOM calculations, and Padé parameters used to test convergence. This material is available free of charge via the Internet at http://pubs.acs.org.

■ AUTHOR INFORMATION

Corresponding Authors

*E-mail: david.wilkins@chem.ox.ac.uk (D. M. Wilkins).
*E-mail: dattani.nike@gmail.com (N. S. Dattani).

Notes

The authors declare no competing financial interest.

■ ACKNOWLEDGMENTS

The results in this publication, and further results, can be found in the 2012 thesis of D.M.W., upon which this article was based. This thesis was completed in partial fulfilment of D.M.W.'s Master of Chemistry degree at the University of Oxford. The authors would like to thank Dmitri Iouchtchenko for careful proofreading of the manuscript. D.M.W. would like to thank the Clarendon Fund and St. Edmund Hall for financial support. N.S.D. thanks the Clarendon Fund, NSERC/CRSNG of/du Canada, and JSPS for financial support; and Yoshitaka Tanimura of Kyoto University for his much appreciated hosting in Kyoto.

■ REFERENCES

(1) Engel, G. S.; Calhoun, T. R.; Read, E. L.; Ahn, T.-K.; Mančal, T.; Cheng, Y.-C.; Blankenship, R. E.; Fleming, G. R. *Nature* **2007**, *446*, 782−786.
(2) Ishizaki, A.; Fleming, G. R. *Proc. Natl. Acad. Sci. U.S.A.* **2009**, *106*, 17255−17260.
(3) Panitchayangkoon, G.; Hayes, D.; Fransted, K. A.; Caram, J. R.; Harel, E.; Wen, J.; Blankenship, R. E.; Engel, G. S. *Proc. Natl. Acad. Sci. U.S.A.* **2010**, *107*, 12766−12770.
(4) Ishizaki, A.; Calhoun, T. R.; Schlau-Cohen, G. S.; Fleming, G. R. *Phys. Chem. Chem. Phys.* **2010**, *12*, 7319−7337.
(5) Collini, E.; Wong, C. Y.; Wilk, K. E.; Curmi, P. M. G.; Brumer, P.; Scholes, G. D. *Nature* **2010**, *463*, 644−647.
(6) Nalbach, P.; Eckel, J.; Thorwart, M. *New J. Phys.* **2010**, *12*, 065043.
(7) Huo, P.; Coker, D. F. *J. Chem. Phys.* **2010**, *133*, 184108.
(8) Scholes, G. D.; Fleming, G. R.; Olaya-Castro, A.; van Grondelle, R. *Nat. Chem.* **2011**, *3*, 763−774.
(9) Yuen-Zhou, J.; Krich, J. J.; Aspuru-Guzik, A. *J. Chem. Phys.* **2012**, *136*, 234501.
(10) Butkus, V.; Valkunas, L.; Abramavicius, D. *J. Chem. Phys.* **2012**, *137*, 044513.
(11) Mančal, T.; Christensson, N.; Lukeš, V.; Milota, F.; Bixner, O.; Kauffmann, H. F.; Hauer, J. *J. Phys. Chem. Lett.* **2012**, *3*, 1497−1502.
(12) Strümpfer, J.; Sener, M.; Schulten, K. *J. Phys. Chem. Lett.* **2012**, *3*, 536−542.

DOI: 10.1021/ct501066k
J. Chem. Theory Comput. XXXX, XXX, XXX−XXX

(13) Christensson, N.; Kauffmann, H. F.; Pullerits, T.; Mančal, T. *J. Phys. Chem. B* **2012**, *116*, 7449−7454.
(14) Kassal, I.; Yuen-Zhou, J.; Rahimi-Keshari, S. *J. Phys. Chem. Lett.* **2013**, *4*, 362−367.
(15) del Rey, M.; Chin, A. W.; Huelga, S. F.; Plenio, M. B. *J. Phys. Chem. Lett.* **2013**, *4*, 903−907.
(16) Mančal, T. *J. Phys. Chem. B* **2013**, *117*, 11282−11291.
(17) Plenio, M. B.; Almeida, J.; Huelga, S. F. *J. Chem. Phys.* **2013**, *139*, 235102.
(18) Fokas, A. S.; Cole, D. J.; Chin, A. W. *Photosynth. Res.* **2014**, *122*, 275−292.
(19) Sato, Y.; Doolittle, B. *J. Chem. Phys.* **2014**, *141*, 185102.
(20) Tempelaar, R.; Jansen, T. L. C.; Knoester, J. *J. Phys. Chem. B* **2014**, *118*, 12865−12872.
(21) Aghtar, M.; Strümpfer, J.; Olbrich, C.; Schulten, K.; Kleinekathöfer, U. *J. Phys. Chem. Lett.* **2014**, *5*, 3131−3137.
(22) Shabani, A.; Mohseni, M.; Rabitz, H.; Lloyd, S. *Phys. Rev. E* **2014**, *89*, 042706.
(23) Pelzer, K. M.; Can, T.; Gray, S. K.; Morr, D. K.; Engel, G. S. *J. Phys. Chem. B* **2014**, *118*, 2693−2702.
(24) Buchleitner, A.; Burghardt, I.; Cheng, Y.; Scholes, G. D.; Schwartz, U. T.; Weber-Bargioni, A.; Wellens, T. *New J. Phys.* **2014**, *16*, 105021.
(25) Mourokh, L. G.; Nori, F.2014, arXiv:1402.7031, arXiv.org ePrint archive, http://arxiv.org/pdf/1402.7031v1.pdf, accessed Feb 10, 2015.
(26) Rivera, E.; Montemayor, D.; Masia, M.; Coker, D. F. *J. Phys. Chem. B* **2013**, *117*, 5510−5521.
(27) Chin, A. W.; Prior, J.; Rosenbach, R.; Caycedo-Soler, F.; Huelga, S. F.; Plenio, M. B. *Nat. Phys.* **2013**, *9*, 113−118.
(28) Jang, S.; Cheng, Y.; Reichmann, D. R.; Eaves, J. D. *J. Chem. Phys.* **2008**, *129*, 101104.
(29) Moix, J.; Wu, J.; Huo, P.; Coker, D.; Cao, J. *J. Phys. Chem. Lett.* **2011**, *2*, 3045−3052.
(30) Wu, J. L.; Liu, F.; Ma, J.; Silbey, R. J.; Cao, J. S. *J. Chem. Phys.* **2012**, *137*, 174111.
(31) Lloyd, S. *J. Phys.: Conf. Ser.* **2011**, *301*, 012037.
(32) Fenna, R. E.; Matthews, B.; Olson, J.; Shaw, E. *J. Mol. Biol.* **1974**, *84*, 231−240.
(33) Fenna, R. E.; Matthews, B. *Nature* **1975**, *258*, 573−577.
(34) Tronrud, D. E.; Wen, J.; Gay, L.; Blankenship, R. E. *Photosynth. Res.* **2009**, *100*, 79−87.
(35) Schmidt am Busch, M.; Muh, F.; El-Amine Madjet, M.; Renger, T. *J. Phys. Chem. Lett.* **2011**, *2*, 93−98.
(36) Schröter, M.; Ivanov, S. D.; Schulze, J.; Polyutov, S. P.; Yan, Y.; Pullerits, T.; Kühn, O. *Phys. Rep.* **2015**, DOI: 10.1016/j.physrep.2014.12.001.
(37) Doolittle, B. Honor's Thesis; Physics and Astronomy Department, Colby College, 2014.
(38) Pachón, L. A.; Brumer, P. *Phys. Chem. Chem. Phys.* **2012**, *14*, 10094−10108.
(39) Lambert, N.; Chen, Y.; Cheng, Y.; Li, C.; Chen, G.; Nori, F. *Nat. Phys.* **2013**, *9*, 10−18.
(40) Zimanyi, E. N.; Silbey, R. J. *J. Chem. Phys.* **2010**, *133*, 144107.
(41) Briggs, J. S.; Eisfeld, A. *Phys. Rev. E* **2011**, *83*, 051911.
(42) Eisfeld, A.; Briggs, J. S. *Phys. Rev. E* **2012**, *85*, 046118.
(43) Miller, W. H. *J. Chem. Phys.* **2012**, *136*, 210901.
(44) León-Montiel, R. de J.; Torres, J. P. *Phys. Rev. Lett.* **2013**, *110*, 218101.
(45) Mančal, T. *J. Phys. Chem. B* **2013**, *117*, 11282−11291.
(46) van Grondelle, R.; Dekker, J. P.; Gillbro, T.; Sundstrom, V. *Biochem. Biophys. Acta* **1994**, *1187*, 1−65.
(47) Scholes, G. D. *Annu. Rev. Phys. Chem.* **2003**, *54*, 57−87.
(48) Renger, T. *Photosynth. Res.* **2009**, *102*, 471−485.
(49) Cheng, Y.-C.; Fleming, G. R. *Annu. Rev. Phys. Chem.* **2009**, *60*, 241−262.
(50) Ishizaki, A.; Fleming, G. R. *J. Chem. Phys.* **2009**, *130*, 234111.
(51) Tao, G.; Miller, W. H. *J. Phys. Chem. Lett.* **2010**, *1*, 891−894.
(52) Ritschel, G.; Roden, J.; Strunz, W. T.; Aspuru-Guzik, A.; Eisfeld, A. *J. Phys. Chem. Lett.* **2011**, *2*, 2912−2917.
(53) Huo, P.; Coker, D. F. *J. Chem. Phys.* **2011**, *135*, 201101.
(54) Zhu, J.; Kais, S.; Rebentrost, P.; Aspuru-Guzik, A. *J. Phys. Chem. B* **2011**, *115*, 1531−1537.
(55) Shabani, A.; Mohseni, M.; Rabitz, H.; Lloyd, S. *Phys. Rev. E* **2012**, *86*, 011915.
(56) Berkelbach, T.; Markland, T.; Reichman, D. *J. Chem. Phys.* **2012**, *136*, 084104.
(57) Seuss, D.; Eisfeld, A.; Strunz, W. *Phys. Rev. Lett.* **2014**, *113*, 150403.
(58) Imai, H.; Ohtsuki, Y.; Kono, H. *Chem. Phys.* **2015**, *446*, 134−141.
(59) Hwang-Fu, Y.; Chen, W.; Cheng, Y. *Chem. Phys.* **2015**, *447*, 46−53.
(60) Louwe, R. J. W.; Aartsma, T. J. *J. Phys. Chem. B* **1997**, *101*, 7221−7226.
(61) Plenio, M. B.; Huelga, S. F. *New J. Phys.* **2008**, *10*, 113019.
(62) Hu, J.; Xu, R.-X.; Yan, Y. *J. Chem. Phys.* **2010**, *133*, 101106.
(63) Hu, J.; Luo, M.; Jiang, F.; Xu, R.-X.; Yan, Y. *J. Chem. Phys.* **2011**, *134*, 244106.
(64) Tanimura, Y. *J. Chem. Phys.* **2014**, *141*, 044144.
(65) Tanimura, Y.; Kubo, R. *J. Phys. Soc. Jpn.* **1989**, *58*, 101−114.
(66) Tanimura, Y. *Phys. Rev. A* **1990**, *41*, 6676−6687.
(67) Tanimura, Y.; Wolynes, P. *Phys. Rev. A* **1991**, *43*, 4131.
(68) Kato, T.; Tanimura, Y. *J. Chem. Phys.* **2002**, *117*, 6221.
(69) Kato, T.; Tanimura, Y. *J. Chem. Phys.* **2004**, *120*, 260.
(70) Tanimura, Y.; Mukamel, S. *J. Chem. Phys.* **1994**, *101*, 3049.
(71) Ishizaki, A.; Tanimura, Y. *J. Chem. Phys.* **2005**, *123*, 014503.
(72) Ishizaki, A.; Tanimura, Y. *J. Chem. Phys.* **2006**, *125*, 084501.
(73) Jin, J.; Welack, S.; Luo, J.; Li, X.-Q.; Cui, P.; Xu, R.-X.; Yan, Y. *J. Chem. Phys.* **2007**, *126*, 134113.
(74) Hein, B.; Kreisbeck, C.; Kramer, T.; Rodríguez, M. *New J. Phys.* **2012**, *14*, 023018.
(75) Han, P.; Xu, R.-X.; Li, B.; Xu, J.; Cui, P.; Mo, Y.; Yan, Y. *J. Phys. Chem. B* **2006**, *110*, 11438.
(76) Schröder, M.; Schreiber, M.; Kleinekathöfer, U. *J. Chem. Phys.* **2007**, *126*, 114102.
(77) Ishizaki, A.; Tanimura, Y. *J. Phys. Soc. Jpn.* **2005**, *74*, 3131−3134.
(78) Ishizaki, A.; Tanimura, Y. *J. Chem. Phys.* **2006**, *125*, 084501.
(79) Yan, Y.-A.; Yang, F.; Liu, Y.; Shao, J. *Chem. Phys. Lett.* **2004**, *395*, 216.
(80) Xu, R.-X.; Cui, P.; Li, X.-Q.; Mo, Y.; Yan, Y. *J. Chem. Phys.* **2005**, *122*, 41103.
(81) Kleinekathöfer, U.; Barvík, I.; Heřman, P.; Kondov, I.; Schreiber, M. *J. Phys. Chem. B* **2003**, *107*, 14094.
(82) Kleinekathöfer, U. *J. Chem. Phys.* **2004**, *121*, 2505.
(83) Yan, Y.; Xu, R. *Annu. Rev. Phys. Chem.* **2005**, *56*, 187.
(84) Jin, J.; Welack, S.; Luo, J.; Li, X.-Q.; Cui, P.; Xu, R.-X.; Yan, Y. *J. Chem. Phys.* **2007**, *126*, 134113.
(85) Dattani, N. S.; Pollock, F. A.; Wilkins, D. M. *Quant. Phys. Lett.* 2012, *1*, 35; http://arxiv.org/abs/1203.4551.
(86) Dattani, N. S.; Wilkins, D. M.; Pollock, F. A. arXiv:1205.4651, 2012; arXiv.org ePrint archive, http://arxiv.org/pdf/1205.4651v2.pdf, accessed May 19, 2015.
(87) Kreisbeck, C.; Kramer, T.; Rodriguez, M.; Hein, B. *J. Chem. Theor. Comput.* **2011**, *7*, 2166.
(88) Hou, D.; Wang, S.; Wang, R.; Ye, L.-Z.; Xu, R.-X.; Zheng, X.; Yan, Y. *J. Chem. Phys.* **2015**, *142*, 104112.
(89) Förster, T. *Ann. Phys.* **1948**, *437*, 55−75.
(90) Yang, M.; Fleming, G. R. *Chem. Phys.* **2002**, *282*, 163−180.
(91) Palmieri, B.; Abramavicius, D.; Mukamel, S. *J. Chem. Phys.* **2009**, *130*, 204512.
(92) Roden, J.; Eisfeld, A.; Wolff, W.; Strunz, W. T. *Phys. Rev. E* **2009**, *103*, 058301.
(93) Rebentrost, P.; Mohseni, M.; Aspuru-Guzik, A. *J. Chem. Phys. B* **2009**, *113*, 9942−9947.
(94) Alicki, R.; Miklaszewski, W. *J. Chem. Phys.* **2012**, *136*, 134103.
(95) Kreisbeck, C.; Kramer, T. *J. Phys. Chem. Lett.* **2012**, *3*, 2828−2833.
(96) Kramer, T.; Kreisbeck, C. *AIP Conf. Proc.* **2014**, *1575*, 111.

DOI: 10.1021/ct501066k
J. Chem. Theory Comput. XXXX, XXX, XXX−XXX

(97) Adolphs, J.; Renger, T. *Biophys. J.* **2006**, *91*, 2778−2797.
(98) Nalbach, P.; Braun, D.; Thorwart, M. *Phys. Rev. E* **2011**, *84*, 041926.
(99) Olbrich, C.; Strümpfer, J.; Schulten, K.; Kleinekathöfer, U. *J. Phys. Chem. Lett.* **2011**, *2*, 1771−1776.
(100) Read, E. L.; Schlau-Cohen, G. S.; Engel, G. S.; Wen, J.; Blankenship, R. E.; Fleming, G. R. *Biophys. J.* **2008**, *95*, 847−856.
(101) Zigmantas, D.; Read, E. L.; Mančal, T.; Brixner, T.; Gardiner, A. T.; Cogdell, R. J.; Fleming, G. R. *Proc. Natl. Acad. Sci. U.S.A.* **2006**, *103*, 12672−12677.
(102) Read, E. L.; Engel, G. S.; Calhoun, T. R.; Mančal, T.; Ahn, T. K.; Blankenship, R. E.; Fleming, G. R. *Proc. Natl. Acad. Sci. U.S.A.* **2007**, *104*, 14203−14208.
(103) Ritschel, G.; Roden, J.; Strunz, W. T.; Eisfeld, A. *New J. Phys.* **2011**, *13*, 113034.

DOI: 10.1021/ct501066k
J. Chem. Theory Comput. XXXX, XXX, XXX−XXX